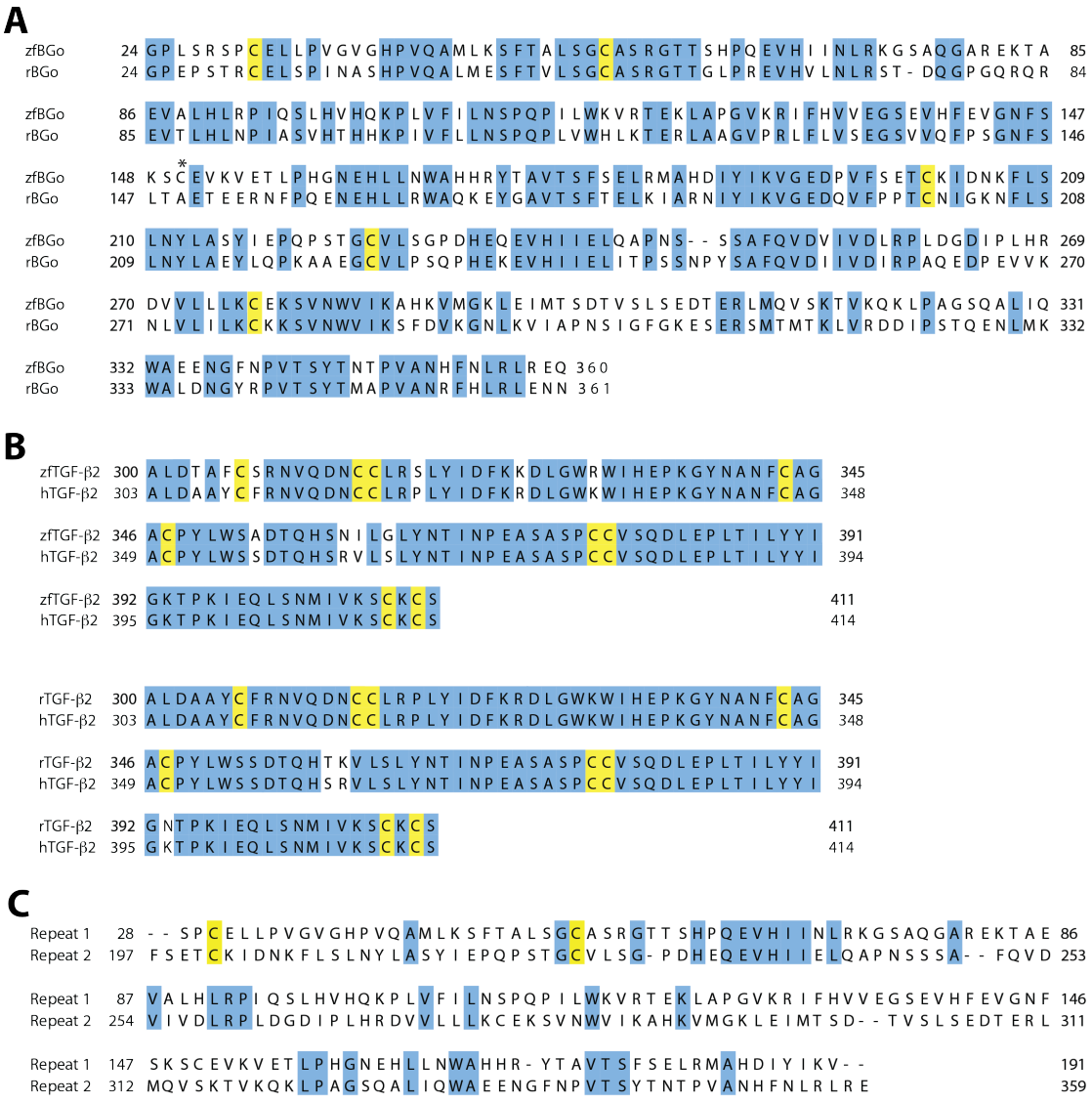

Figure S1. Related to Figures 3 and 4. Sequence alignments of betaglycan and TGF-β. A. Sequence alignment of zfBG$_O$ and rBG$_O$. Colored residues indicate those that are identical between the two proteins (overall amino acid identity is 181/336, or 53.9 %). Cysteines are highlighted in yellow, all other residues in blue. Cysteine residue present in zfBG$_O$, but not rBG$_O$, is highlighted by an asterisk (*). B. Sequence alignment of the growth factor domain of zebrafish and human TGF-β2 and rat and human TGF-β2. Colored residues indicate those that are identical between the two proteins (overall amino acid identity is 102/112, or 91.1 % for zfTGF-β2 and hTGF-β2 and 109/112, or 97.3 % for rTGF-β2 and hTGF-β2). Cysteines are highlighted in yellow, all other residues in blue. C. Sequence alignment of the repeating element found in zebrafish betaglycan orphan domain. Repeating element is defined as an "exit" sequence, followed by the complete sequence of the β-sandwich domain that follows. Repeating elements 1 and 2 correspond to residues 28 – 191 and 197-359, respectively. Colored residues indicate those that are identical between the two proteins (overall amino acid identity 32/160, or 20.0 %). Cysteines are highlighted in yellow, all other residues in blue. Sequences were aligned in all cases with the program Clustal Omega (Sievers et al., 2011) and were rendered with the program Jalview (Waterhouse et al., 2009). Residue numbering in all cases is relative to the N-terminal methionine of the natural signal peptide (signal peptide not shown).

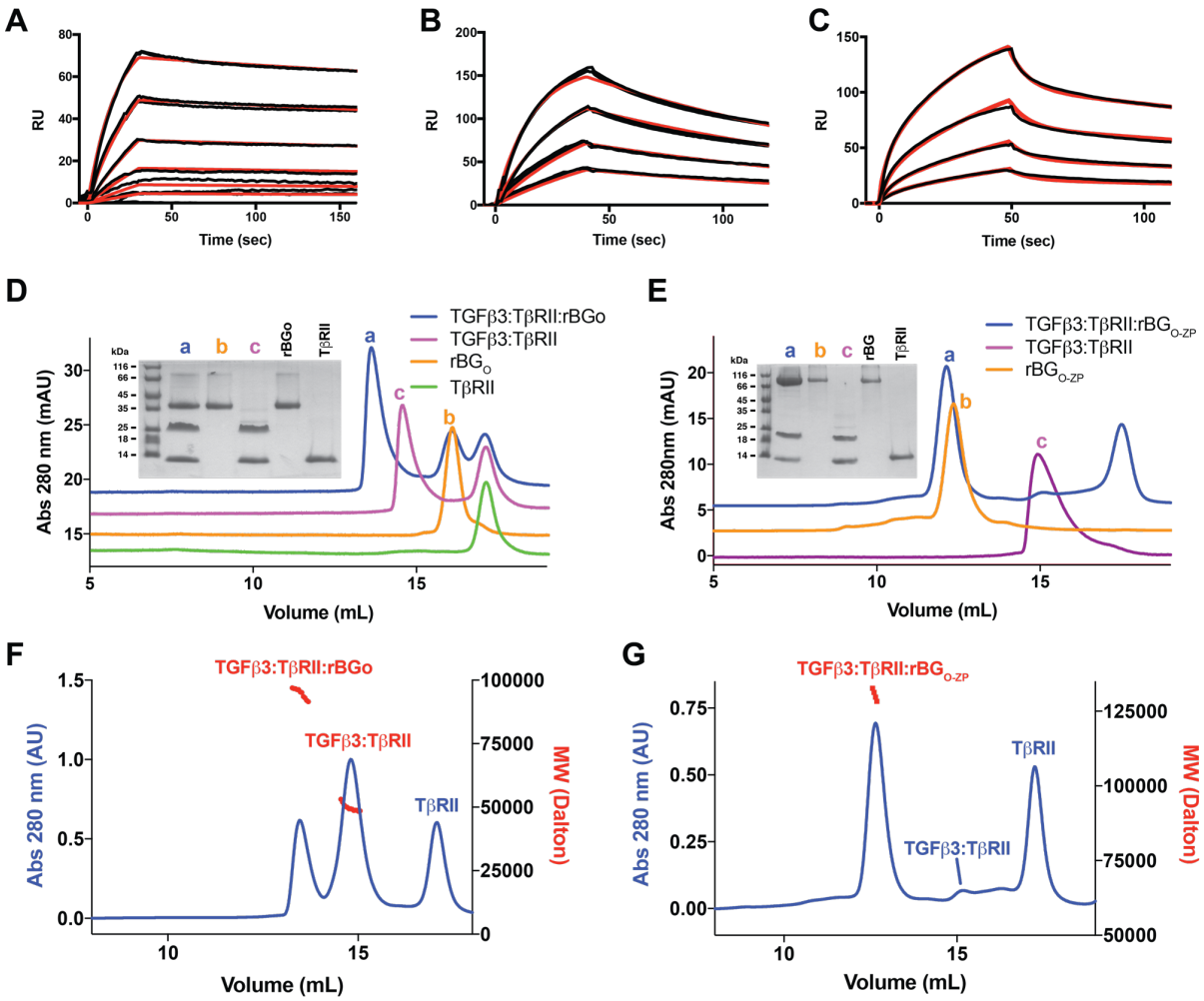

Figure S2. Related to Figure 2. Characterization of rat betaglycan binding to TGF-β2. A-C. SPR sensorgrams of rat full-length betaglycan (rBG$_{O-ZP}$) (A), rat betaglyan orphan domain (rBG$_O$) (B), and rat ZP-C domain (rBG$_{ZP-C}$) (C) binding to immobilized TGF-β2. Kinetic fit is shown in red over the experimental curves shown in black. **D-E.** Complexes formed between rBG$_O$ (D) and rBG$_{O-ZP}$ (E) with TGF-β3 and TβRII in solution as assessed using SEC; for panel D, the TGF-β3:TβRII:rBG$_O$ ternary complex is shown in blue, the TGF-β3:TβRII binary complex in magenta, and TβRII and rBG$_O$ alone in green and orange, respectively; for panel E, the TGF-β3:TβRII:rBG$_{O-ZP}$ ternary complex is shown in blue, the TGF-β3:TβRII binary complex in magenta, and rBG$_{O-ZP}$ alone in orange. Shown in the insets are non-reducing SDS-PAGE gels of the major peaks that eluted. **F-G.** SEC-MALS analysis of TGF-β3:TβRII:rBG$_O$ and TGF-β3:TβRII:rBG$_{O-ZP}$ ternary complexes, with the blue trace corresponding to the UV absorbance and the red data points the molecular mass. Observed/anticipated masses for the TGF-β2DM:TβRII:rBG$_O$ and TGF-β2DM:TβRII:rBG$_{O-ZP}$ complexes are 94.9 kDa/91.1 kDa and 129 kDa/123 kDa, respectively.

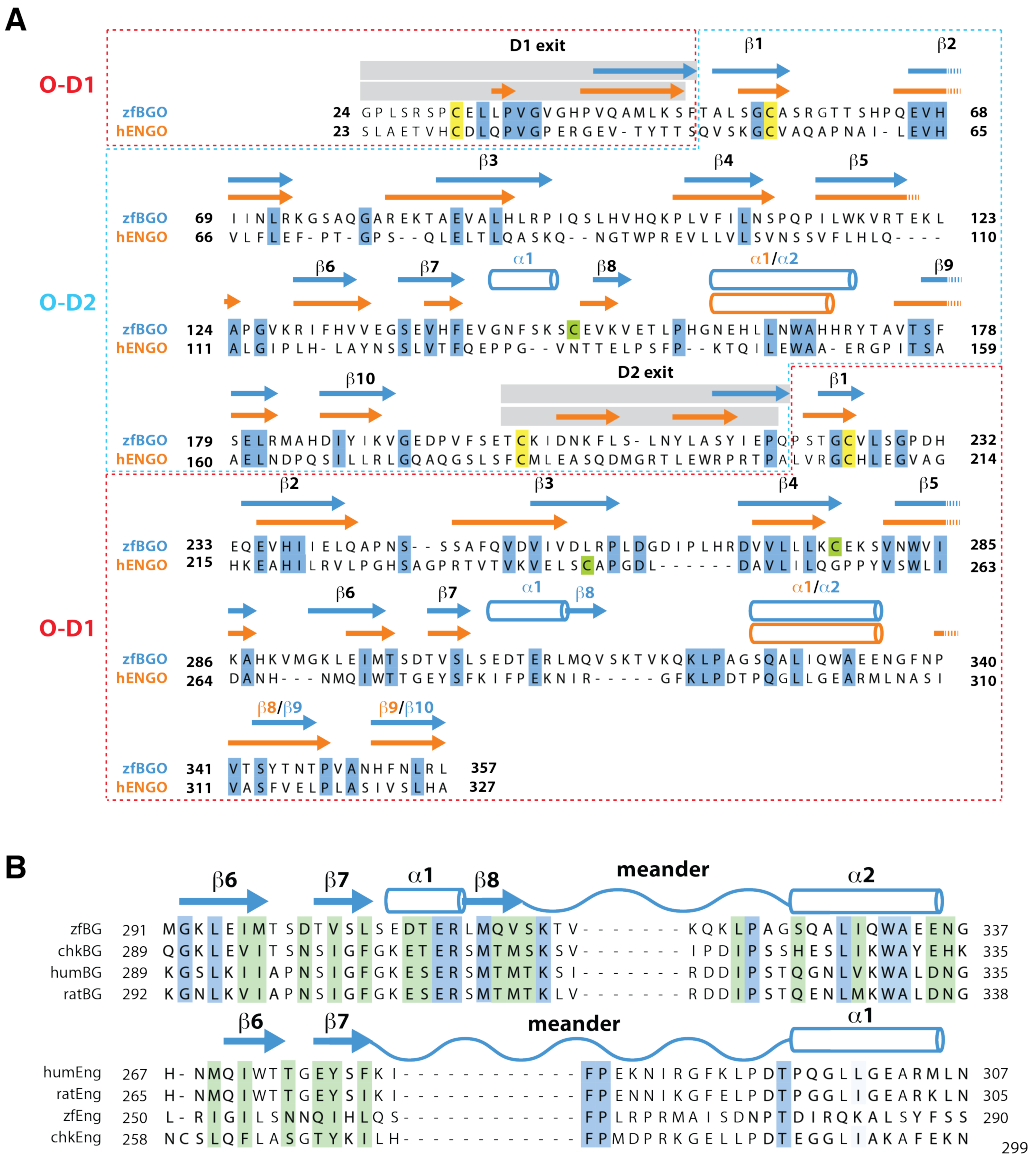

Figure S3. Related to Fig. 4. Sequence alignment of ENG$_O$ and BG$_O$. A. Sequences of hENG$_O$ and zfBG$_O$ were aligned with the program Clustal Omega (Sievers et al., 2011) and were rendered with the program Jalview (Waterhouse et al., 2009). Residues highlighted by blue shading indicate those that are identical between the two proteins (overall amino acid identity is 68/334, or 20.4 %). Cysteines that are conserved between hENG$_O$ and zfBG$_O$ are highlighted in yellow, while cysteines that are not conserved are highlighted in green. Secondary structure elements are shown, as are the sequences corresponding to the O-D1 and O-D2 exits. Dashed red and cyan lines delineate the O-D1 and O-D2 subdomains, respectively. Residue numbering is relative to the N-terminal methionine of the natural signal peptide (signal peptide not shown). **B.** Sequence alignment of BG$_O$ and ENG$_O$ from various species in the region of the β6-contact site previously reported for human ENG and BMP-9 (3). Sequences of zfBG$_O$ and hENG$_O$ were first aligned based on their structures; the remainder of the BGs and ENGs from different species were then aligned to the zfBG$_O$ and hENG$_O$, respectively, using Clustal Omega (1) and then the whole alignment was rendered using Jalview (2). Residues shaded blue are identical between the proteins shown, while those shaded green are conserved. Secondary structure shown along the top of the BG and ENG sequences correspond to those derived from the zfBG$_O$ and hENG$_O$ structures.

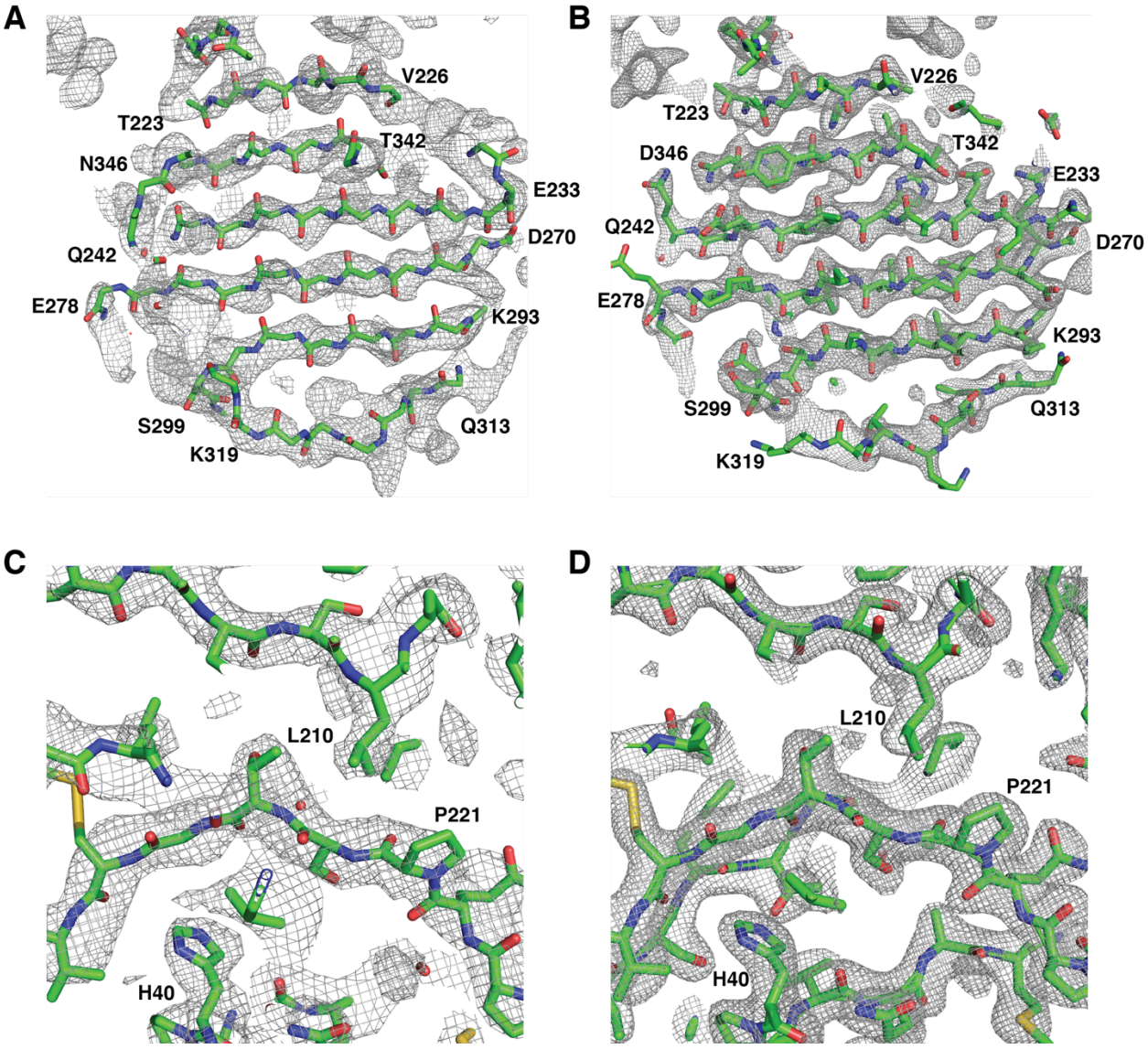

Fig. S4. Related to Figure 3. Experimental and refined electron density for orthorhombic form of zfBG$_O$. A, C. Solvent-flattened experimental electron density map as calculated with the program FFT (Ten Eyck, 1973) using FOM-weighted combined phases. Map shown in panel A corresponds to the convex layer of the D1 β-sandwich and includes the backbone atoms of the final model. Map shown in panel C corresponds to the D2 exit sequence as it re-enters D1 and includes all atoms of the final model. **B, D.** 2mFo-DFc electron density map as calculated using phenix.maps (Adams, et al. 2010) with a bulk solvent correction and anisotropic scaling. Regions shown in panels B and D correspond to those shown in panels A and C and includes all atoms of the final model. Maps in all panels were contoured at 1.2 σ and were displayed using pymol (DeLano, 2019).

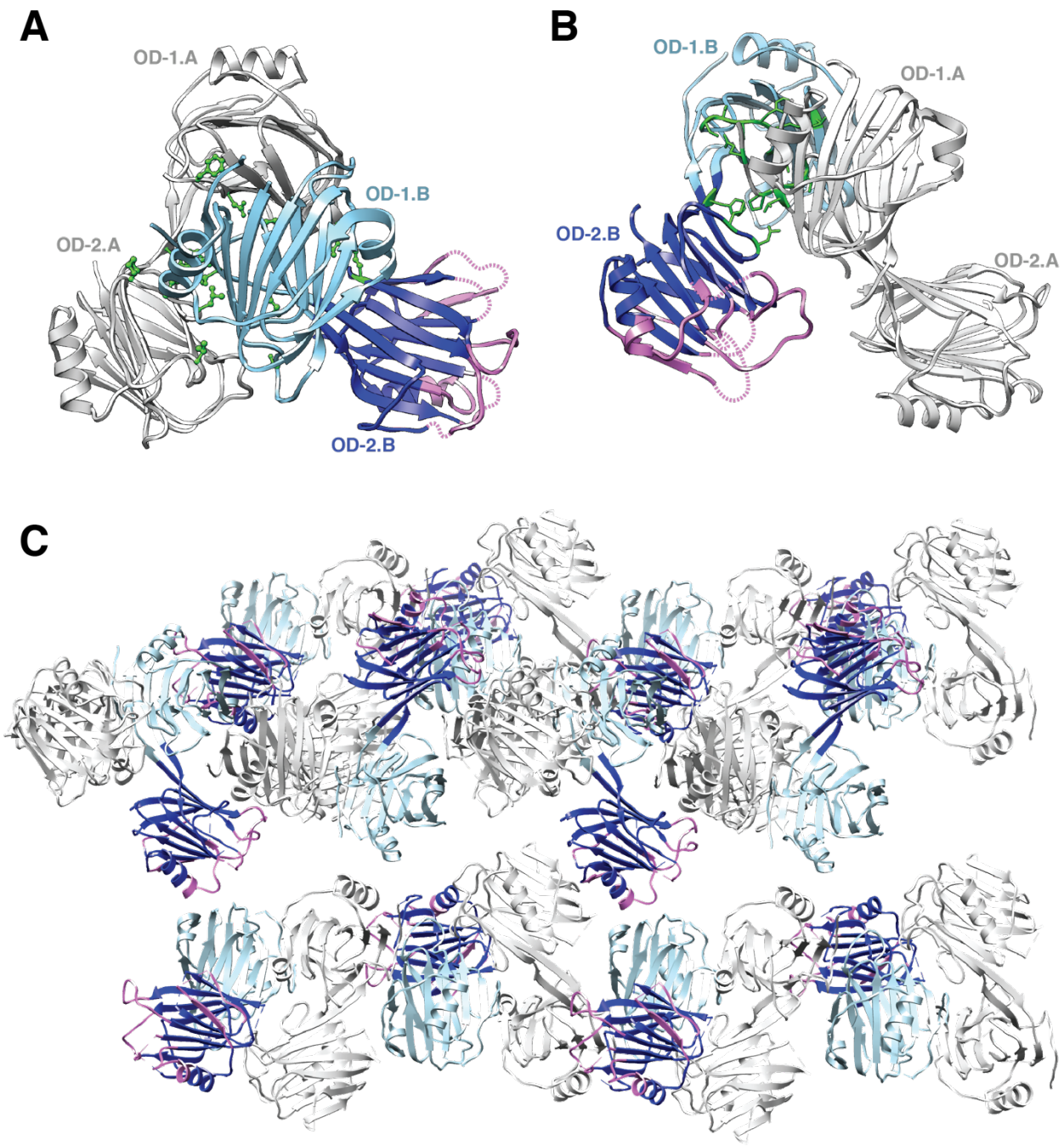

Fig. S5. Related to Figure 3. Crystal packing for the zfBG$_O$ orthorhombic form. A-B. Major lattice contacts for the zfBG$_O$ orthorhombic form as identified using the program PDBePISA (Krissinel and Henrick, 2007). In panel A, the two chains that comprise the crystallographic asymmetric unit are shown to interact, with domain 1 of chain B (OD-1.B, light blue) packing between domains 1 and 2 of chain A (OD-1.A and OD-2.A, shaded grey). In panel B, domain 1 of chain A (OD-1.A, grey) from one asymmetric unit is shown to interact with domain 1 of chain B (OD-1.B, light blue) from an adjacent asymmetric unit. For panels A and B major interface residues are displayed and are shaded green; domain 2 of chain B (OD-2.B) is shaded dark blue, except for regions that are found in regions of weak electron density, which are shaded magenta. C. Expanded view of the orthorhombic lattice with the same shading for chains A and B OD-1 and OD-2 as in panels A and B; OD-1.B (dark blue with magneta) is shown to fall into a solvent void with little to no contact with surrounding chains.

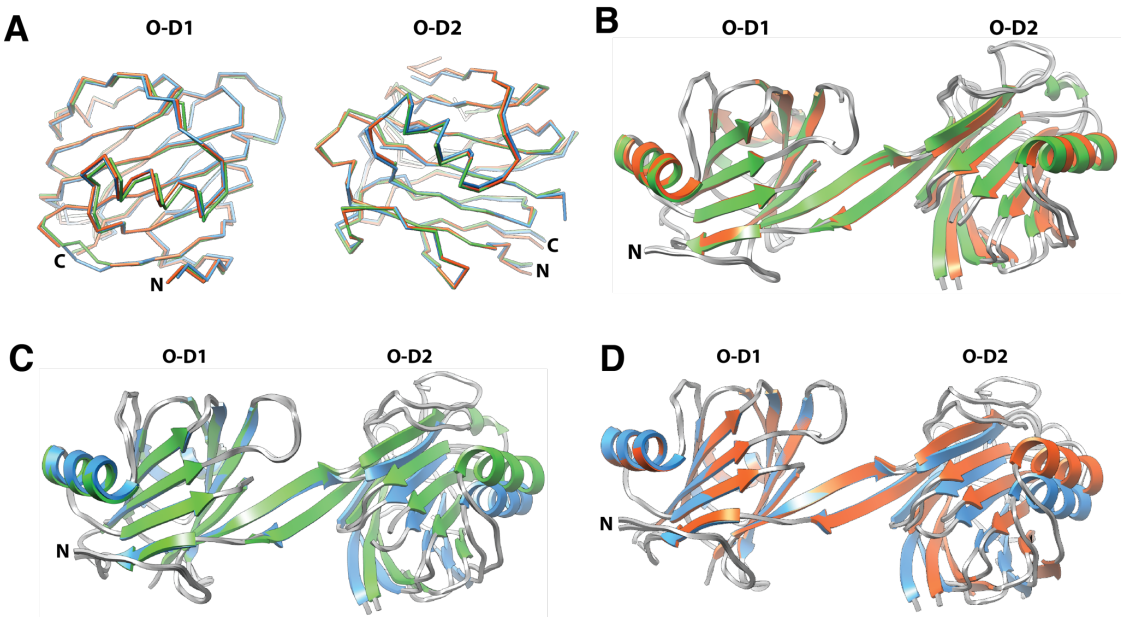

Figure S6. Related to Figure 3. Comparison of different crystal forms of zfBG$_O$. A. Overlay of Cα-traces of the O-D1 and O-D2 domain from the two molecules in the zfBG$_O$ orthorhombic crystal form (chain A orange, chain B blue) and one molecule from the zfBG$_O$ tetragonal crystal form (green). Pairwise RMSDs for all atoms range from 0.78 – 0.83 Å for O-D1 and 0.47 – 0.66 Å for O-D2. **B-C.** Overlays of one of the molecules from the orthorhombic crystal form with the one molecule from the tetragonal crystal form (panel B chain A or panel C chain B). **D.** Overlay of Chain A and Chain B from the orthorhombic crystal form. Overlays in panels B-D were performed by only minimizing differences for backbone atoms in the O-D1 subdomain. Models shown in panels B-D are shaded in the same manner as panel A.

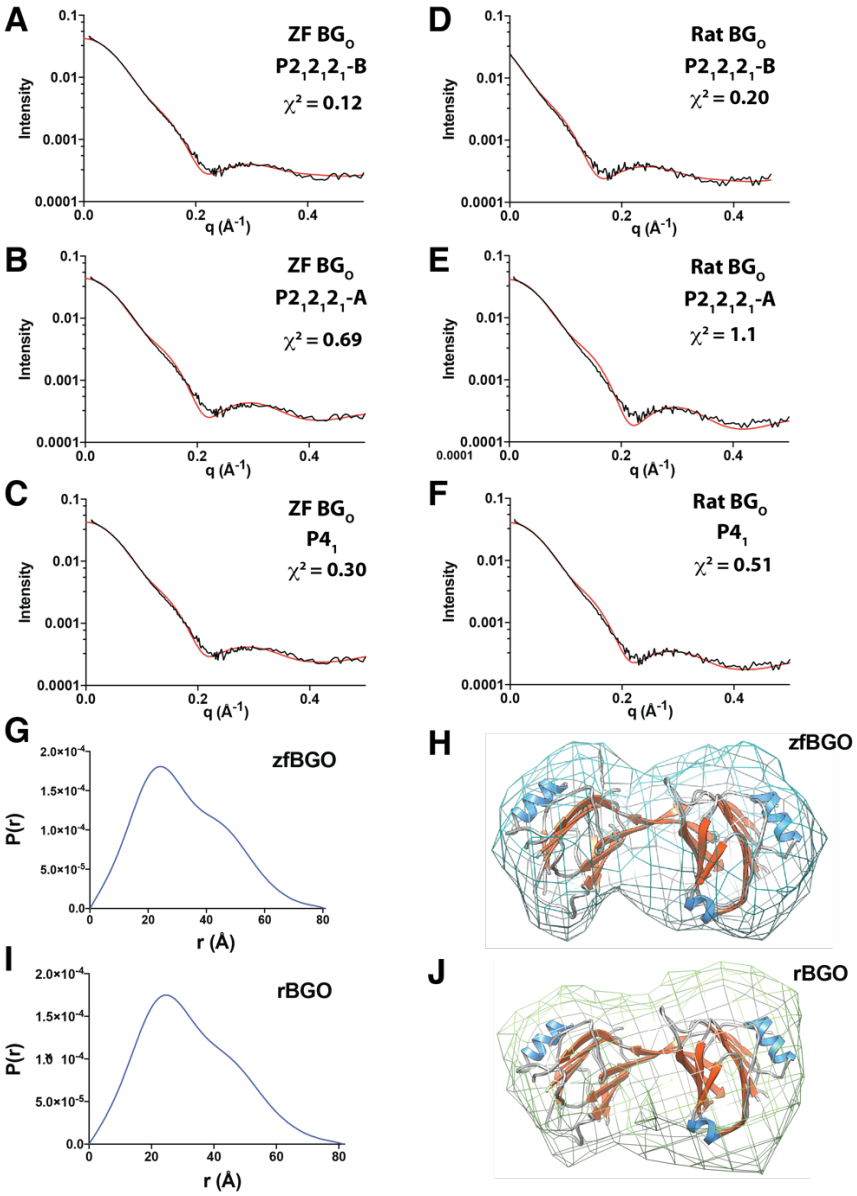

Figure S7. Related to Figure 3. Correspondence of zfBG$_O$ crystal structures with zfBGo and rBG$_O$ solution structures. A-F. SAXS curves (black traces) for zebrafish (A-C) and rat (D-F) betaglycan orphan domains, together with the best fit scattering curves (red traces) and chi squared values calculated with the program Crysol (Svergun, et al., 1995) from chain B of the zfBG$_O$ orthorhombic crystal structure (A, D), chain A of the zfBG$_O$ orthorhombic crystal structure (B, E), or zfBG$_O$ tetragonal crystal structure (C, F). **G, I.** P(r) distance distribution curves for zfBG$_O$ (G) and rBG$_O$ (I). The major peak and shoulder at 25 and 47 Å in the P(r) distance distribution functions correspond well with the mean diameter for O-D1 and O-D2 (24.3 Å) and the interdomain distance (48.4 Å). **H, J.** Calculated electron density maps contoured at 1.5 sigma for zfBG$_O$ and rBG$_O$ (H and J, respectively) with the structure of zfBG$_O$ from the orthorhombic form chain B fitted into the density. Estimated resolution of the zfBG$_O$ and rBG$_O$ maps from Fourier shell correlation analysis is 32.8 and 26.3 Å, respectively.

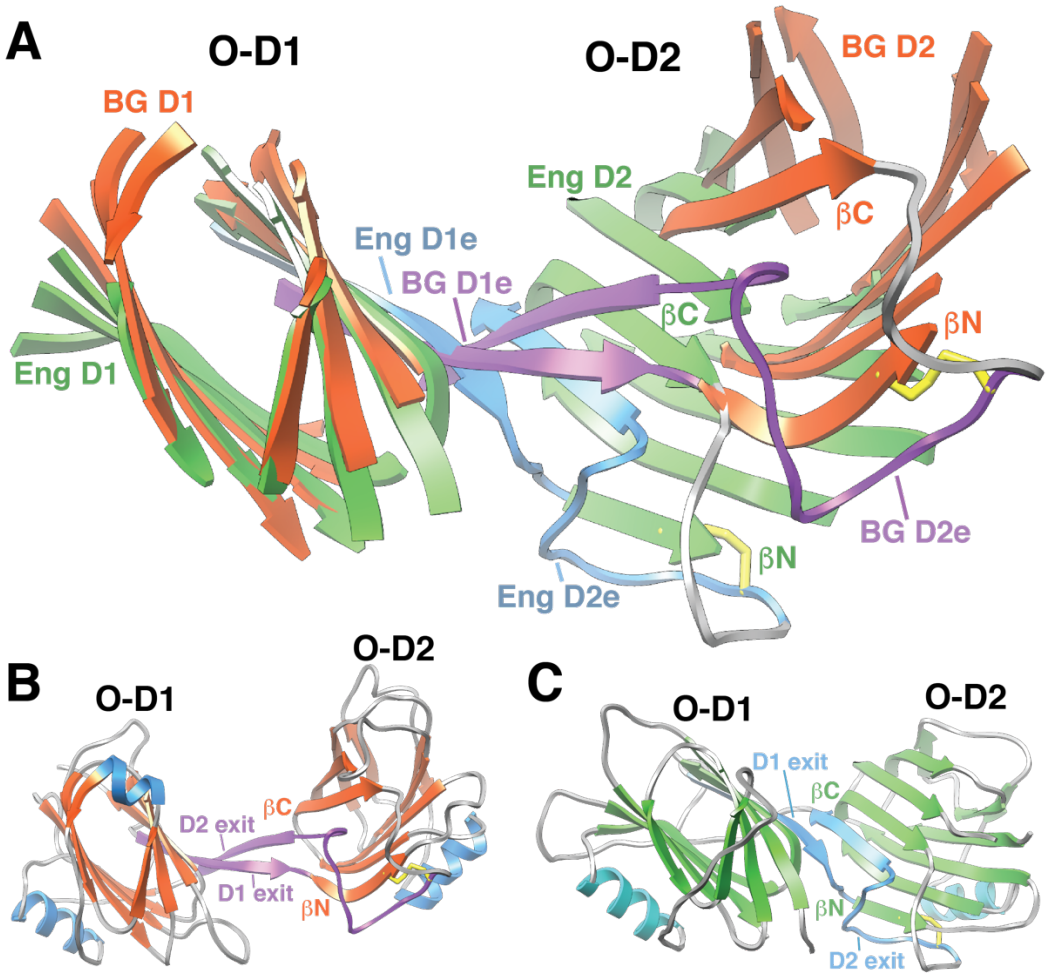

Figure S8. Related to Figure 4. Relative domain orientations differ in $zfBG_O$ and $hENG_O$. A. An overlay of $zfBG_O$ and $hENG_O$ in which only the atomic positions in O-D1 have been minimized. All loop regions and helices have been omitted for clarity. $zfBG_O$ β-strands and exit sequences (D1e and D2e) are shaded orange and purple, respectively. $hENG_O$ β-strands and exit sequences (D1e and D2e) are shaded green and blue, respectively. **B-C.** $zfBG_O$ and $hENG_O$ structures as in panel A, but shown separately (A, $zfBG_O$; B, $hENG_O$) with all loops and helices present.

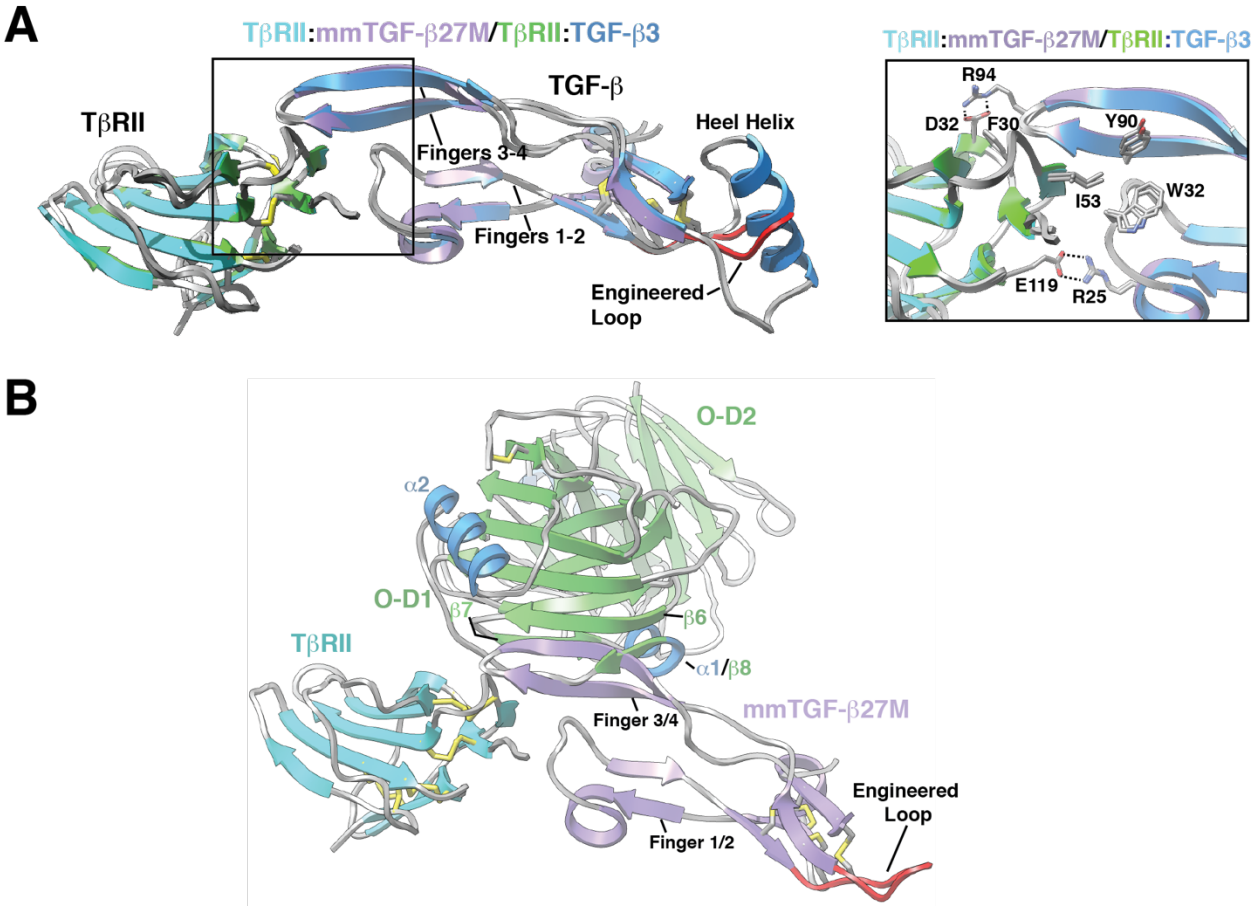

Figure S9. Related to Figure 5. Structure of the 2:1 ENG$_O$:BMP-9 complex and anticipated complex of zfBG$_O$ with mmTGF-β27M. A. Overlay of the 1.8 Å crystal structure of mmTGF-β2-7M:TβRII complex (PDB 5TX4, mmTGF-β2-7M and TβRII shown in lavender and cyan ribbons, respectively) (Kim, et al, 2017) with one of the TGF-β3 monomers and its bound TβRII from the 3.0 Å crystal structure of the TGF-β3:TβRII:TβRI complex (PDB 2PJY, TGF-β3 monomer and TβRII shown in blue and green ribbon, respectively; TβRI not shown for clarity) (Groppe, et al, 2008). Newly created loop in mmTGF-β2 (red) which takes the place of the heel (α3) helix in TGF-β2 is depicted in red. Expansion on the right shows the nearly the same conformations for critical hydrophobic and hydrogen-bonding/electrostatic interactions in the mmTGF-β2-7M:TβRII and TGF-β3:TβRII stuctures shown to be essential for high affinity TGF-β3:TβRII binding (Baardsnes, et al, 2009; DeCrescenzo, et al, 2006). **B.** Putative endoglin-like manner of zfBG$_O$ binding to the mmTGF-β27M:TβRII binary complex. Model was constructed by aligning the mmTGF-β27M part of the mmTGF-β27M:TβRII complex to one of the BMP-9 monomers in the crystal structure of the 2:1 hENG$_O$:BMP-9 complex (PDB 5HZW) (Saito, et al, 2017) and zfBG$_O$ to the corresponding bound hENG$_O$ molecule in the same complex. mmTGF-β27M is depicted in lavender, with its engineered loop in red, TβRII in cyan, and zfBG$_O$ in green (β-strands) and blue (helices). Panel A is adapted from Kim, et. al, *J. Biol. Chem*., 292, 7173-7188 (2017).

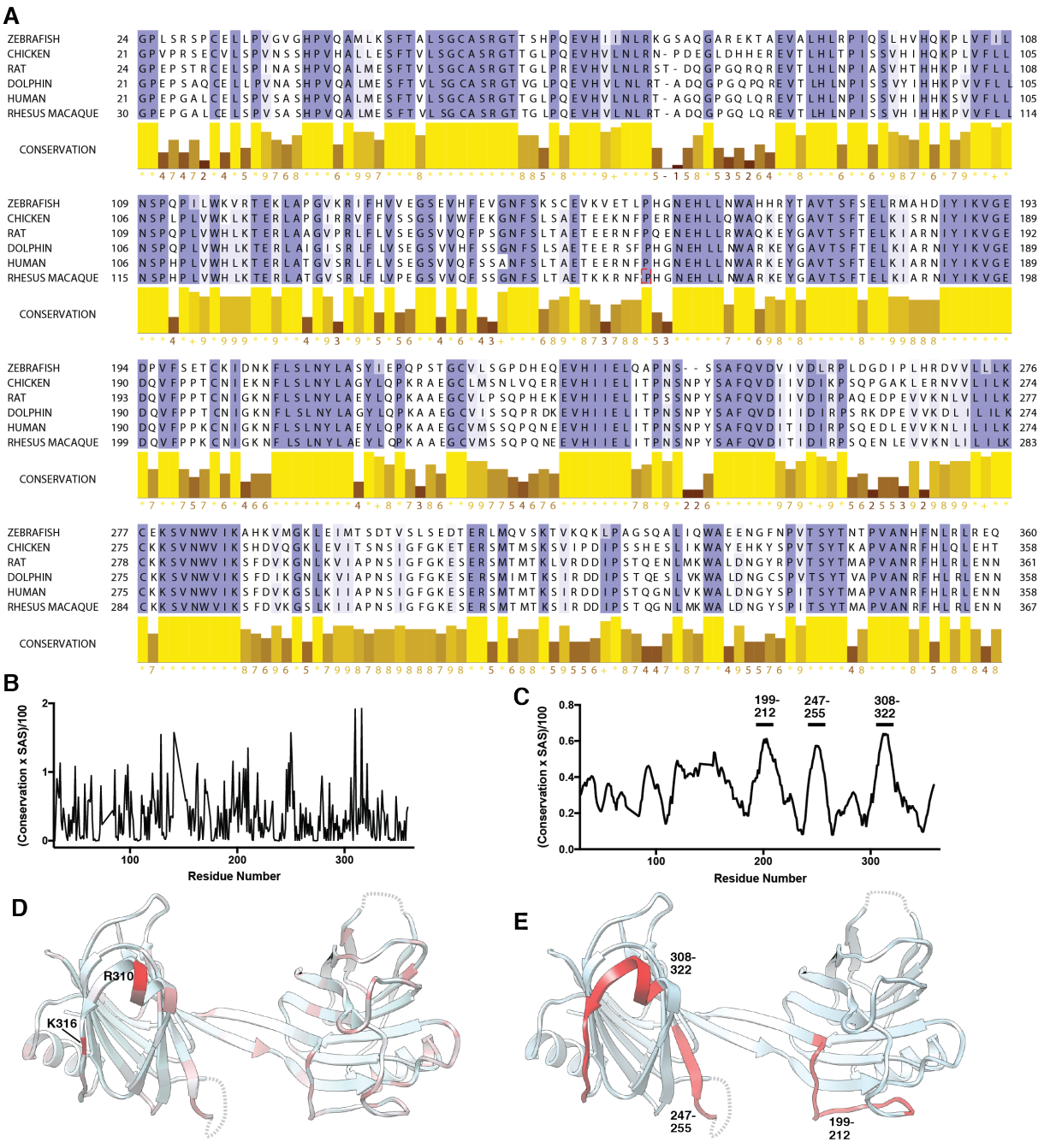

Fig. S10. Related to Figure 7. Conserved surfaced exposed residues of BG$_O$. A. An alignment of BG$_O$ from six different species, with residues shaded by increasing levels of conservation (lowest conservation light blue, highest conservation dark blue). Numeric conservation index is shown below in yellow. Sequences were aligned using Clustal Omega (Sievers et al., 2011) and were rendered with Jalview (Waterhouse et al., 2009). **B, C.** Plot of the conservation index, times the solvent accessible surface area, divided by 100 as a function of the residue number; panel C is the same as panel B, but smoothed over a 10-residue sliding window. **D.** Structure of zfBG$_O$ shaded according to the conservation/solvent accessible surface area index shown in panel B (light blue corresponds to an index of 0, while red corresponds to an index of 2.0). **E.** Structure of zfBG$_O$ shaded red to highlight the three regions with the highest continuous conservations/solvent accessible surface area, residues 199-212, 247-255, and 308-322.

Table S1. Related to STAR*METHODS. Growth factor constructs used in this study

Construct	Residue range, features, and plasmid used for expression[1]	Amino Acid Sequence
TGF-β2	Residues 303-414 of human TGF-β2 (NCBI NP_003229) Plasmid: Hincklab #225	ALDAAYCFRNVQDNCCLRPLYIDFKRDLGWKWIH EPKGYNANFCAGACPYLWSSDTQHSRVLSLYNTINP EASASPCCVSQDLEPLTILYYIGKTPKIEQLSNMIVKS CKCS
TGF-β2DM	Residues 303-414 of human TGF-β2 (NCBI NP_003229) K327R and K396R substitutions (red) enable high affinity T□RII binding Plasmid: Hincklab #253	ALDAAYCFRNVQDNCCLRPLYIDFRRDLGWKWIH EPKGYNANFCAGACPYLWSSDTQHSRVLSLYNTINP EASASPCCVSQDLEPLTILYYIGRTPKIEQLSNMIVKS CKCS
TGF-β2TM	Residues 303-414 of human TGF-β2 (NCBI NP_003229) K327R, I394V, and K396R substitutions (red) enable high affinity TβRII binding Plasmid: Hincklab #225	ALDAAYCFRNVQDNCCLRPLYIDFRRDLGWKWIH EPKGYNANFCAGACPYLWSSDTQHSRVLSLYNTINP EASASPCCVSQDLEPLTILYYVGRTPKIEQLSNMIVK SCKCS
mmTGF-β2-7M	Residues 303-352 and 377-414 of mouse TGF-β2 (NCBI NP_0033393) connected by an engineered loop (blue) C379S substitution (magenta) renders the protein monomeric; K327R, R328K, L391V, I394V, K396R, T397K, and I400V substitutions (red) enable high affinity TβRII binding Plasmid: Hincklab #267	ALDAAYCFRNVQDNCCLRPLYIDFRKDLGWKWIH EPKGYNANFCAGACPYRASKSPSCVSQDLEPLTIVY YVGRKPKVEQLSNMIVKSCKCS
avi-mmTGF-β2-7M	Residues 303-352 and 377-414 of mouse TGF-β2 (NCBI NP_0033393) connected by an engineered loop (blue); Avi-tag (orange) appended onto the N-terminus C379S substitution (magenta) renders the protein monomeric; K327R, R328K, L391V, I394V, K396R, T397K, and I400V	MGLNDIFEAQKIEWHEEFALDAAYCFRNVQDNCC LRPLYIDFRKDLGWKWIHEPKGYNANFCAGACPYR ASKSPSCVSQDLEPLTIVYYVGRKPKVEQLSNMIVK SCKCS

	substitutions (red) enable high affinity TβRII binding Plasmid: Hincklab #273	
TGF-β3	Residues 301-412 of human TGF-β3 (NCBI NP_003230) Plasmid: Hincklab #27	ALDTNYCFRNLEENCCVRPLYIDFRQDLGWKWVH EPKGYYANFCSGPCPYLRSADTTHSTVLGLYNTLN PEASASPCCVPQDLEPLTILYYVGRTPKVEQLSNMV VKSCKCS

[1]All residue numbering begins with the N-terminal methionine of the naturally occurring signal peptide

Table S2. Related to STAR*METHODS. Receptor constructs used in this study

Construct	Residue range and features[1]	Sequence
TβRII	Residues 38-153 of human TβRII (NCBI NP_003233) Plasmid: Hincklab #249	VTDNNGAVKFPQLCKFCDVRFSTCDNQKSCMSNCS ITSICEKPQEVCVAVWRKNDENITLETVCHDPKLPY HDFILEDAASPKCIMKEKKKPGETFFMCSCSSDECN DNIIFSEEY
zfBG$_{O\text{-}ZP}$	Residues 24-774 of zfBG (NCBI NP_001298101) Rat serum albumin signal peptide (red) appended on the N-terminus Hexahistidine tag (blue) appended on the C-terminus S522A substitution (magenta) eliminates glycos-aminoglycan (GAG) attachment site Plasmid: Hincklab #305	MKWVTFLLLLFISGSAFSAAA GPLSRSPCELLPVGVGHPVQAMLKSFTALSGCASRG TTSHPQEVHIINLRKGSAQGAREKTAEVALHLRPIQS LHVHQKPLVFILNSPQPILWKVRTEKLAPGVKRIFHV VEGSEVHFEVGNFSKSCEVKVETLPHGNEHLLNWAH HRYTAVTSFSELRMAHDIYIKVGEDPVFSETCKIDNK FLSLNYLASYIEPQPSTGCVLSGPDHEQEVHIIELQAP NSSSAFQVDVIVDLRPLDGDIPLHRDVVLLLKCEKSV NWVIKAHKVMGKLEIMTSDTVSLSEDTERLMQVSK TVKQKLPAGSQALIQWAEENGFNPVTSYTNTPVANH FNLRLREQVSDVGIMDEGMLPPFSILRNINPLPKPSAR DAPPRNGFPFPFLPMDQDQSFPPLMPPHEDSVFLAGG PEEHQGSADVGFNVQCEKNKMVVSIEKETLQANGFG KPNITLQDSQCKATSNATHYILETPLSGCQTSKIPSHP SPVVLYINAIVISQSEQKDGAGWPVDDEDMEPGEVLL PGDALPELTERILPVNGHHATILFNCTYRKNQDSPFD TDAGSDDFLVDSTANVTFNMELYNNHFQFPNSQPFL TVTENRPVFVEIAATKADPNLGFMIQTCFISPDSNPA VQSEYVVIENICPKDDSVVYYPQRGDFPIPHAQMDK KRFSFTYRSKFNVSLLFLHCEMSLCSRRNDKEMNLA ECMLPDEACTSLSIESILLIMMNTKTLTKPIVVISDDM PVTVKVPWDESPPRQGHHHHHH
zfBG$_{O}$	Residues 29-359 of zfBG (NCBI NP_001298101) Rat serum albumin signal peptide (red) appended on the N-terminus Hexahistidine tag (blue) appended on the C-terminus Plasmid: Hincklab #309	MKWVTFLLLLFISGSAFSAAA GSPCELLPVGVGHPVQAML KSFTALSGCASRGTT SHPQEVHIINLRKGSAQGAREKTAEVALHLRPIQSLH VHQKPLVFILNSPQPILWKVRTEKLAPGVKRIFHVVE GSEVHFEVGNFSKSCEVKVETLPHGNEHLLNWAHHR YTAVTSFSELRMAHDIYIKVGEDPVFSETCKIDNKFLS LNYLASYIEPQPSTGCVLSGPDHEQEVHIIELQAPNSSS AFQVDVIVDLRPLDGDIPLHRDVVLLLKCEKSVNWVI KAHKVMGKLEIMTSDTVSLSEDTERLMQVSKTVKQK LPAGSQALIQWAEENGFNPVTSYTNTPVANHFNLRLR EHHHHHH
zfBG$_{ZP\text{-}C}$	Residues 587-757 of zfBG (NCBI NP_001298101) Rat serum albumin signal peptide (red) appended on the N-terminus Hexahistidine tag (blue) appended on the C-terminus	MKWVTFLLLLFISGSAFSAAA GSSTANVTFNMELYNNHFQFPNSQPFLTVTENRPVFV EIAATKADPNLGFMIQTCFISPDSNPAVQSEYVVIENI CPKDDSVVYYPQRGDFPIPHAQMDKKRFSFTYRSKFN VSLLFLHCEMSLCSRRNDKEMNLAECMLPDEACTSL SIESILLIMMNTKTLTKPIVVISDDHHHHHH

	Plasmid: Hincklab #310	
zfBG$_{O\text{-}D1}$	Residues 29-48 and 216-359 of zfBG (NCBI NP_001298101) connected with a Thr-Asp dipeptide (magenta) Human serum albumin signal peptide (red) and human albumin (light blue), followed by a thrombin cleavage site (green) appended on the N-terminus Hexahistidine tag (blue) appended on the C-terminus Plasmid: Hincklab #391	MVWVTFISLLFLFSSAYSRGVFRRDAHHHHHHKSEVA HRFKDLGEENFKALVLIAFAQYLQQCPFEDHVKLVNE VTEFAKTCVADESAENCDKSLHTLFGDKLCTVATLRE TYGEMADCCAKQEPERNECFLQHKDDNPNLPRLVRP EVDVMCTAFHDNEETFLKKYLYEIARRHPYFYAPELLF FAKRYKAAFTECCQAADKAACLLPKLDELRDEGKASS AKQRLKCASLQKFGERAFKAWAVARLSQRFPKAEFAE VSKLVTDLTKVHTECCHGDLLECADDRADLAKYICEN QDSISSKLKECCEKPLLEKSHCIAEVENDEMPADLPSLA ADFVESKDVCKNYAEAKDVFLGMFLYEYARRHPDYS VVLLLRLAKTYETTLEKCCAAADPHECYAKVFDEFKP LVEEPQNLIKQNCELFEQLGEYKFQNALLVRYTKKVP QVSTPTLVEVSRNLGKVGSKCCKHPEAKRMPCAEDYL SVVLNQLCVLHEKTPVSDRVTKCCTESLVNRRPCFSA LEVDETYVPKEFNAETFTFHADICTLSEKERQIKKQTA LVELVKHKPKATKEQLKAVMDDFAAFVEKCCKADDK ETCFAEEGKKLVAASQVALGLGSTSGSGAQTNASSGT LVPRGSGSPCELLPVGVGHPVQAMLKSTDYIEPQSTG CVLSGPDHEQEVHIIELQAPNSSSAFQVDVIVDLRPLD GDIPLHRDVVLLLKCEKSVNWVIKAHKVMGKLEIMT SDTVSLSEDTERLMQVSKTVKQKLPAGSQALIQWAEE NGFNPVTSYTNTPVANHFNLRLREHHHHHH
zfBG$_{O\text{-}D2}$	Residues 50-216 of zfBG (NCBI NP_001298101) Rat serum albumin signal peptide (red) appended on the N-terminus Hexahistidine tag (blue) appended on the C-terminus Plasmid: Hincklab #392	MKWVTFLLLLFISGSAFSAAA TALSGCASRGTTSHPQEVHI INLRKGSAQGAREKTA EVALHLRPIQSLHVHQKPLVFILNSPQPILWKVRTEK LAPGVKRIFHVVEGSEVHFEVGNFSKSCEVKVETLP HGNEHLLNWAHHRYTAVTSFSELRMAHDIYIKVGE DPVFSETCKIDNKFLSLNYLASYHHHHHH
rBG$_{O\text{-}ZP}$	Residues 31-759 of rBG (NP_058952) Rat serum albumin signal peptide (red) appended on the N-terminus Hexahistidine tag (blue) appended on the C-terminus S535A and S546A substitutions (magenta) eliminates glycos-aminoglycan (GAG) attachment sites Plasmid: Hincklab #276	MKWVTFLLLLFISGSAFSAAA CELSPINASHPVQALMESFTVLSGCASRGTTGLPREVH VLNLRSTDQGPGQRQREVTLHLNPIASVHTHHKPIVFL LNSPQPLVWHLKTERLAAGVPRLFLVSEGSVVQFPSGN FSLTAETEERNFPQENEHLLRWAQKEYGAVTSFTELKI ARNIYIKVGEDQVFPPTCNIGKNFLSLNYLAEYLQPKA AEGCVLPSQPHEKEVHIIELITPSSNPYSAFQVDIIVDIR PAQEDPEVVKNLVLILKCKKSVNWVIKSFDVKGNLK VIAPNSIGFGKESERSMTMTKLVRDDIPSTQENLMKW ALDNGYRPVTSYTMAPVANRFHLRLENNEEMRDEEV HTIPPELRILLDPDHPPALDNPLFPGEGSPNGGLPFPFP DIPRRGWKEGEDRIPRPKQPIVPSVQLLPDHREPEEVQ GGVDIALSVKCDHEKMVVAVDKDSFQTNGYSGMEL TLLDPSCKAKMNGTHFVLESPLNGCGTRHRRSTPDG VVYYNSIVVQAPSPGDSAGWPDGYEDLEAGDNGFPG DGDEGETAPLSRAGVVVFNCSLRQLRNPSGFQGQLDG

		NATFNMELYNTDLFLVPSPGVFSVAENEHVYVEVSVT KADQDLGFAIQTCFLSPYSNPDRMSDYTIIENICPKDDS VKFYSSKRVHFPIPHAEVDKKRFSFLFKSVFNTSLLFLH CELTLCSRKKGSLKLPRCVTPDDACTSLDATMIWTMM QNKKTFTKPLAVVLQVDHHHHHH
rBG$_O$	Residues 31-361 of rBG (NP_058952) Rat serum albumin signal peptide (red) appended on the N-terminus Hexahistidine tag (blue) appended on the C-terminus Plasmid: Hincklab #281	MKWVTFLLLLFISGSAFSAAA CELSPINASHPVQALMESFTVLSGCASRGTTGLPREVH VLNLRSTDQGPGQRQREVTLHLNPIASVHTHHKPIVFL LNSPQPLVWHLKTERLAAGVPRLFLVSEGSVVQFPSGN FSLTAETEERNFPQENEHLLRWAQKEYGAVTSFTELKI ARNIYIKVGEDQVFPPTCNIGKNFLSLNYLAEYLQPKA AEGCVLPSQPHEKEVHIIELITPSSNPYSAFQVDIIVDIR PAQEDPEVVKNLVLILKCKKSVNWVIKSFDVKGNLK VIAPNSIGFGKESERSMTMTKLVRDDIPSTQENLMKW ALDNGYRPVTSYTMAPVANRFHLRLENNHHHHHH
rBG$_{ZP-C}$	Residues 590-757of rBG (NP_058952) Rat serum albumin signal peptide (red) appended on the N-terminus Hexahistidine tag (blue) appended on the C-terminus Plasmid: Hincklab #282	MKWVTFLLLLFISGSAFSAAA GNATFNMELYNTDLFLVPS PGVFSVAENEHVYVEVS VTKADQDLGFAIQTCFLSPYSNPDRMSDYTIIENICPK DDSVKFYSSKRVHFPIPHAEVDKKRFSFLFKSVFNTSL LFLHCELTLCSRKKGSLKLPRCVTPDDACTSLDATMIW TMMQNKKTFTKPLAVVLQHHHHHH

[1]All residue numbering begins with the N-terminal methionine of the naturally occurring signal peptide

Table S3. Related to Figure 3. Regions with weak electron density that could not be reliably modeled

Crystal Form	Chain	Residues
$P2_12_12_1$	A	75-83, 144-146, 229-230, 246-247
$P2_12_12_1$	B	61-65, 76-83, 121-128, 142-148, 198-200, 232-233
$P4_1$	A	75-83, 142-151, 173-174